RSC Advances

PAPER

View Article Online
View Journal | View Issue

Cite this: *RSC Adv.*, 2021, **11**, 1282

Optimal fluorescence and photosensitivity properties of dual-functional $NaYb_{1-x}F_4:Tm_x^{3+}$ nanoparticles for applications in imaging guided photodynamic therapy†

Zhang Jiayin,[a] Wang Qiyu,*[b] Liang Hong,[a] Song Guoli*[a] and Zhang Zhiguo*[c]

Received 10th November 2020
Accepted 20th December 2020

DOI: 10.1039/d0ra09544c

rsc.li/rsc-advances

The fluorescence and photosensitivity properties of $NaYb_{1-x}F_4:Tm_x^{3+}$ nanoparticles were optimized to develop noninvasive near-infrared fluorescence imaging-guided photodynamic therapy. The emission at 800 nm from Tm^{3+} presented an exponential increase with an increase in the Tm^{3+} doping concentration from 0 to 2%. The photosensitivity properties of $NaYb_{1-x}F_4:Tm_x^{3+}$ nanoparticles were also studied *via* the chemoprobe method, which used a reactive oxygen quencher, 1,3-diphenylisobenzofuran (DPBF). With the increase in the doping concentration of Tm^{3+}, the generation rate of reactive oxygen species in $NaYb_{1-x}F_4:Tm_x^{3+}$ nanoparticles decreased linearly at a rate of 0.3. The doping concentration of Tm^{3+} had two opposite effects on the 800 nm emission and generation rates of reactive oxygen species. The competitive relationship was discussed and an optimal value for the Tm^{3+} doping concentration of approximately 1% was determined. At this concentration, the energy of the Yb^{3+} excited state can be fully utilized, and the fluorescence and photosensitivity properties are an effective combination.

Introduction

Photodynamic therapy (PDT), due to its highly specific selectivity and minimal invasiveness, has become an intriguing route for treating tumors.[1–3] In typical PDT, the photosensitizer (PS) is excited by light and generates reactive oxygen species (ROS), killing tumor cells with minimal damage to surrounding tissues. PSs are key components in the implementation of effective PDT.[4,5] Generally, traditional PSs need to be excited by visible light, which results in poor penetration depth in tissue, due to which their use is limited to the superficial treatment of tumors.[6,7] A tissue is known to have a biological window in the near infrared light (NIR) region from 800 to 1100 nm, as the excitation light in this range exhibits weak scattering and absorption in the tissue, enabling deep penetration. Efforts have been invested to extend the excitation wavelengths of PSs to the NIR range. For instance, two-photon-excited PSs have been developed.[8–10] Unfortunately, the absorption cross-section of two-photon-excited PSs is too small, necessitating the use of a high-energy pulse laser, which significantly exceeds safe limits for clinical applications. Upconversion nanoparticle (UCNP)-based PSs, which feature UCNP-loaded traditional PSs (NPs-PSs) to perform PDT, are proposed as alternative candidates. Specifically, UCNPs absorb NIR light and emit visible light to trigger traditional PSs to generate ROS.[11–13] In the process, severe relaxation losses and low upconversion efficiencies lead to an impractically low ROS quantum yield. Recently, we proposed an NIR-excited inorganic PS, $NaYbF_4$ NPs, that could achieve NIR-excited PDT with high efficiencies *via* a simple energy transfer method.[14] In addition, $NaYbF_4$ NPs serve as PSs directly without drug loading and release, making the therapeutic effect more controllable and stable. However, $NaYbF_4$ NPs are difficult to guide to the positions of tumor due to the weak emission of Yb^{3+}. Therefore, it is imperative to introduce a luminescence element to $NaYbF_4$ NPs for achieving precise tumor localization and high-efficiency PDT.

In this study, we design a novel nanocomposite $NaYb_{1-x}F_4:Tm_x^{3+}$ as the PS for application to imaging-guided PDT. The fluorescence characteristics and ROS generation were investigated in detail using $NaYb_{1-x}F_4:Tm_x^{3+}$ NPs. The energy distribution relationship between the 800 nm fluorescence intensity and ROS generation rate was obtained. Next, the energy distribution between imaging and PDT was adjusted by changing the Tm^{3+} doping concentration, and an optimal value for the Tm^{3+} doping concentration was determined at which fluorescence and photosensitivity properties combined effectively.

[a]School of Technology, Harbin University, Harbin 150086, China. E-mail: SONGGL@aliyun.com

[b]School of Physics & Electronic Engineering, Harbin Normal University, Harbin 150025, China. E-mail: hsdwqy@126.com

[c]School of Instrumentation Science and Engineering, Harbin Institute of Technology, Harbin 150080, P. R. China. E-mail: zhangzhiguo@hit.edu.cn

† Electronic supplementary information (ESI) available. See DOI: 10.1039/d0ra09544c

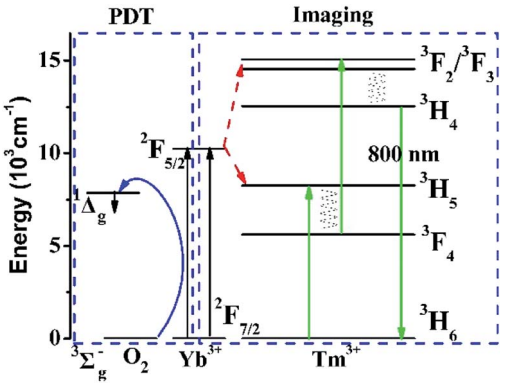

Fig. 1 Energy levels of Yb^{3+}, Tm^{3+}, and O_2 systems and the proposed energy transition mechanisms for the 800 nm upconversion emission and generation of ROS.

Results and discussion

To explain the energy transfer mechanism of $NaYb_{1-x}F_4:Tm_x^{3+}$ as a PS, the energy level diagrams of the Yb^{3+}, Tm^{3+}, and O_2 systems are shown in Fig. 1. On the one hand, Yb^{3+} absorbs NIR excitation light, and passes on part of its energy to Tm^{3+} *via* two successive energy transfer processes to populate the $^3F_{2,3}$ states of Tm^{3+}. Next, the population in the $^3F_{2,3}$ states relaxes to the $^3H_4$ state *via* the nonradiative relaxation process. Moreover, the population in the $^3H_4$ state decays radiatively to the ground state, resulting in the NIR emission band at approximately 800 nm.[15] On the other hand, excited Yb^{3+} can directly transfer part of their energy to oxygen to generate ROS *via* a simple energy transfer process. Therefore, the $NaYb_{1-x}F_4:Tm_x^{3+}$ NPs are very suitable as PSs for imaging-guided PDT.

A typical TEM image and a low-magnification TEM image of $NaYb_{99\%}F_4:Tm_{1\%}^{3+}$ are shown in Fig. 2a and S1,† respectively. A histogram of the NP size distribution was obtained using the Nano Measurer 1.2.5 software by calculating the size of NPs in the TEM bright-field image (Fig. 2b). The mathematical details regarding the calculation of the particle size distribution are presented in Table S1.† The mean NP size is approximately 6.5 nm. The XRD pattern of $NaYb_{99\%}F_4:Tm_{1\%}^{3+}$ NPs was obtained, and the positions of the diffraction peaks were found to closely match the JCPDS-PDF 77-2043 cubic phase of $NaYbF_4$ NPs (Fig. 2c). Furthermore, the effect of the Tm^{3+} doping concentration on the structure of $NaYb_{1-x}F_4:Tm_x^{3+}$ NPs was investigated through XRD analysis using specimens with Tm^{3+} concentrations of 1% and 2%, as shown in Fig. S2.† No distinct difference was observed between the diffraction angles for Tm^{3+} concentrations at 1% and 2%. It is probably due to similar radii of 0.0858 nm and 0.087 nm for Yb^{3+} and Tm^{3+}, respectively. A low doping concentration would not cause a marked change in the crystal lattice. Liang *et al.* conducted a similar study. They found that when the Yb^{3+} concentration in $NaYb_{98\%}F_4:Tm_{2\%}^{3+}$ is approximately 98%, the XRD pattern is consistent with the JCPDS standard card.[16]

Fig. 3a presents the fluorescence spectra of $NaYb_{1-x}F_4:Tm_x^{3+}$ (x = 1, 2, 3, 4) NPs. Further, the integrated intensities of the 800 nm emission with different Tm^{3+} doping concentrations are shown intuitively in Fig. 3b. The intensity of the 800 nm emission is observed to initially increase. When the doping concentration of Tm^{3+} reaches 2%, the fluorescence intensity of 800 nm is at its maximum. As the doping concentration of Tm^{3+} continues to increase, the fluorescence intensity at 800 nm begins to decrease due to Tm^{3+} concentration quenching. In this study, we consider the Tm^{3+} concentration to be within 2%. The detailed relationship between the fluorescence intensity and Tm^{3+} concentration is explored. The typical fluorescence spectra of $NaYb_{1-x}F_4:Tm_x^{3+}$ (x = 0.2, 0.5, 1, 1.5, 2) NPs are shown in Fig. 3c. Fig. 3d shows the 800 nm fluorescence intensities of $NaYb_{1-x}F_4:Tm_x^{3+}$ NPs at different Tm^{3+} concentrations. We used the average value and standard deviation of the 800 nm emission for three-repeats of measurement, as shown in Fig. S3,† which was normalized by the intensity for 2% Tm^{3+}. The normalized 800 nm fluorescence intensities of $NaYb_{1-x}F_4:Tm_x^{3+}$ NPs were enhanced exponentially with the Tm^{3+} doping concentration (x) in the form of $y = 1 - \exp(-x/x_0)$, which is shown in Fig. 3d. Although $x_0 = 0.6\%$ is the optimized Tm^{3+} doping concentration for the fluorescence intensity, it is not the optimum concentration for dual functions (imaging and PDT).

To theoretically investigate the effect of the Tm^{3+} concentration on the intensity of the 800 nm emission, the rate equations in the steady states based on the energy transitions were studied through eqn (S1)–(S5).† As illustrated in eqn (S5),† the same pump power density was utilized to excite the 800 nm emissions; hence, ρ is a constant parameter for all the samples. The absorption cross-sections of the Yb^{3+} ions are similar. N_{Yb0} can be regarded as constant because the concentration of Yb^{3+} only exhibits a small change. Therefore, eqn (S5)† can be simplified as follows:

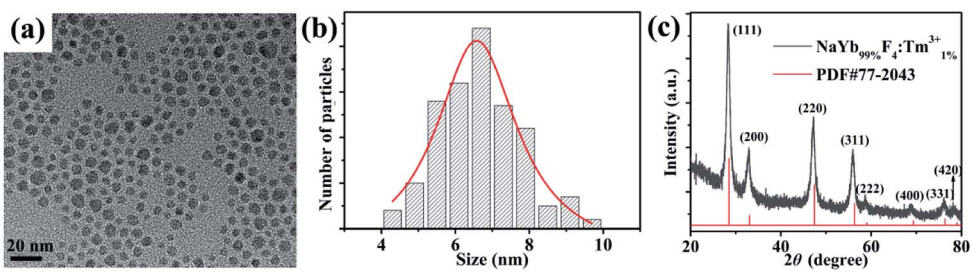

Fig. 2 (a) Typical TEM image of $NaYb_{1-x}F_4:Tm_x^{3+}$ (x = 1%) NPs; (b) size distribution of $NaYb_{99\%}F_4:Tm_{1\%}^{3+}$ NPs; (c) corresponding XRD pattern.

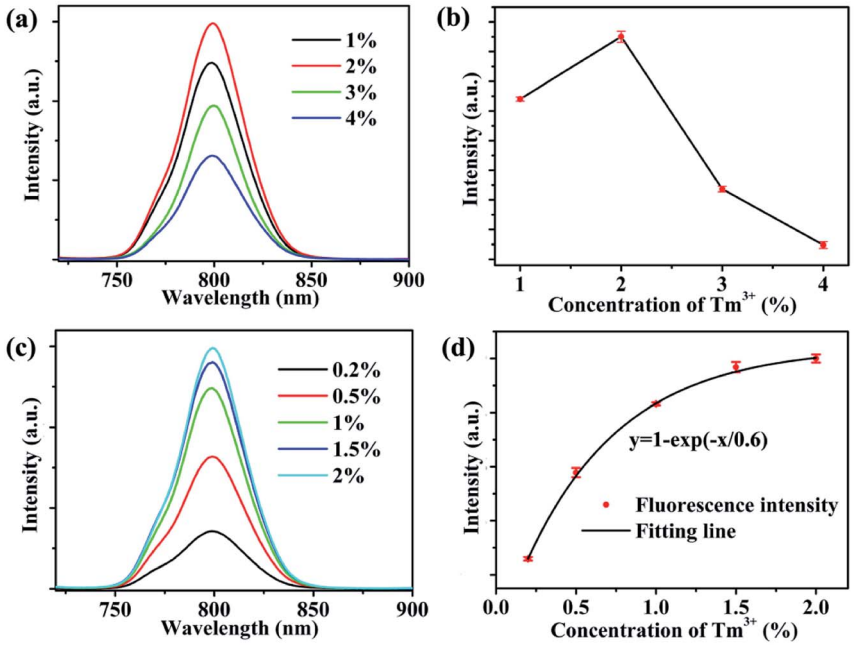

Fig. 3 (a) 800 nm emission spectra of $NaYb_{1-x}F_4:Tm_x^{3+}$ ($x = 1, 2, 3, 4\%$); (b) fluorescence intensity with Tm^{3+} concentration over a wide range; (c) 800 nm emission spectra of $NaYb_{1-x}F_4:Tm_x^{3+}$ ($x = 0.2, 0.5, 1, 1.5, 2\%$); (d) relationship between fluorescence intensity and Tm^{3+} concentration for a narrow range.

$$I_{800} \propto W_0 W_1 N_0 \tau_{Yb1}{}^2 \tau_1 \quad (1)$$

The intensity of the 800 nm emission in eqn (1) is related to: the energy transfer rate between Yb^{3+} and Tm^{3+} ions (W_i); the population densities of the ground state (N_0) in Tm^{3+}; and the decay times of Yb^{3+} in excited states (τ_{Yb1}) and Tm^{3+} in $^3F_4$ states (τ_1). When the Tm^{3+} concentration increases, W_0, W_1, and N_0 in eqn (1) increase. On the contrary, with increasing Tm^{3+} concentration, the distance between the Tm^{3+} ions decreases and cross-relaxation is enhanced, leading to a decrease in τ_{Yb1} and τ_1.[16–18] At low concentrations of Tm^{3+}, the rates of increase for W_0, W_1, and N_0 are higher than the rate of decrease for $\tau_{Yb1}{}^2\tau_1$; hence, the intensity of the 800 nm emission increases with increasing Tm^{3+} concentration. As the Tm^{3+} concentration continues to increase, the decrease in $\tau_{Yb1}{}^2\tau_1$ is faster than the increases in W_0, W_1, and N_0. This is probably because the values of τ_{Yb1} and τ_1 are very small and $\tau_{Yb1}{}^2\tau_1$ decreases rapidly due to the power function and product form. Therefore, the intensity of the 800 nm emission decreases at a high Tm^{3+} concentration.

Furthermore, we studied the relationship between singlet oxygen generation and the Tm^{3+} doping concentration. The 1,3-diphenylisobenzofuran (DPBF) absorbance spectra of $NaYb_{1-x}F_4:Tm_x^{3+}$ ($x = 0.2, 0.5, 1, 1.5, 2\%$) were measured three times (Fig. S4†). Fig. 4a displays the normalized DPBF absorbance as a function of the irradiation time in the $NaYb_{1-x}F_4:Tm_x^{3+}$ NP solutions. The absorbance shows an exponential decay with the light exposure time. Next, the consumption rate of DPBF as an indicator of ROS generation rate was determined by the slope of linear fitting,[19] as shown in the inset of Fig. 4a. Fig. 4b shows the consumption rates of DPBF at different Tm^{3+} concentrations, which use the average value and standard deviation for three-repeats of measurement and are normalized

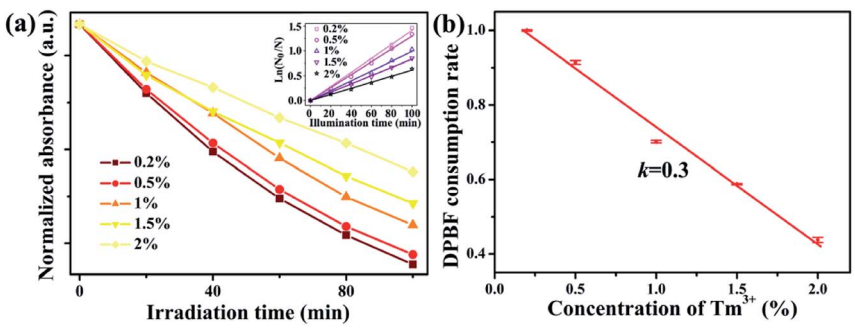

Fig. 4 (a) DPBF absorbance at 410 nm *versus* exposure time and consumption rates of DPBF under different Tm^{3+} concentrations in $NaYb_{1-x}F_4:Tm_x^{3+}$ ($x = 0.2, 0.5, 1, 1.5, 2\%$); (b) relationship between DPBF consumption rate and Tm^{3+} concentration in $NaYb_{1-x}F_4:Tm_x^{3+}$ ($x = 0.2, 0.5, 1, 1.5, 2\%$).

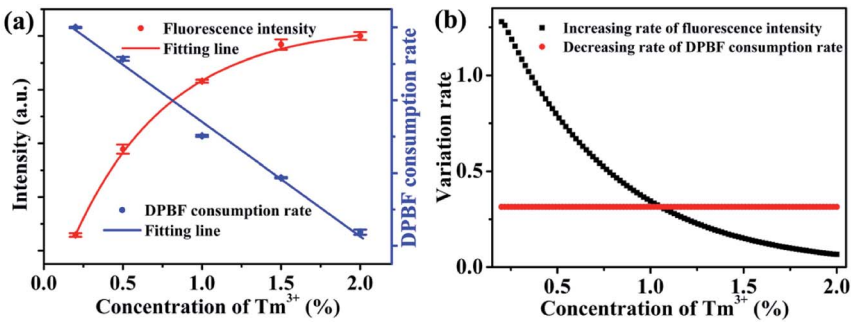

Fig. 5 (a) Fluorescence intensity and DPBF consumption rate with Tm^{3+} concentration in $NaYb_{1-x}F_4:Tm_x^{3+}$ (x = 0.2, 0.5, 1, 1.5, 2%); (b) variation rate of fluorescence intensity and DPBF consumption rate at different Tm^{3+} concentrations in $NaYb_{1-x}F_4:Tm_x^{3+}$ (x = 0.2, 0.5, 1, 1.5, 2%).

by the intensity of Tm^{3+} of 0.2%. At low Tm^{3+} concentrations (0.2–2%), the consumption rates of DPBF decrease linearly at a rate of 0.3 as the Tm^{3+} concentration increases.

For the application of dual-functional $NaYb_{1-x}F_4:Tm_x^{3+}$ NPs, the energy competition mechanism between fluorescence and ROS generation from Yb^{3+} in the excited state should be considered. The Tm^{3+} doping concentration has opposite effects on the fluorescence and ROS generation (Fig. 5a). On the one hand, an increase in the Tm^{3+} doping concentration would facilitate a strong 800 nm upconversion emission. On the other hand, an increased Tm^{3+} doping concentration is unfavorable for a high ROS generation rate. Considering the two opposing effects, an optimum Tm^{3+} doping concentration is required to balance the energy distribution between fluorescence and ROS generation. Here, the variation rate (rate of decrease or increase) of ROS generation and fluorescence intensity can be employed to evaluate the relative rate of variations at different Tm^{3+} doping concentrations. The variation rate can be determined by the derivation of the curves in Fig. 5a. The variation rates of fluorescence intensity and ROS generation are shown in Fig. 5b. The decreasing rate of ROS-generating efficiency is 0.3, which is a constant. Furthermore, the rate of increase of fluorescence intensity decreases exponentially. When the Tm^{3+} doping concentration is less than 1%, the rate of increase for fluorescence intensity is greater than the rate of decrease for ROS generation. Therefore, the improvement in the fluorescence intensity is worth the loss of ROS generation. However, when the Tm^{3+} concentration exceeds 1%, the increasing rate of fluorescence intensity is less than the decreasing rate of ROS generation. Hence, there is an optimal value for the Tm^{3+} concentration, which corresponds to approximately 1%. At this concentration, the energy of the Yb^{3+} excited state can be fully utilized, allowing for the most efficient manner of energy distribution.

Experimental

Synthesis of NPs

$NaYb_{1-x}F_4:Tm_x^{3+}$ (x = 0.2, 0.5, 1, 1.5, 2%, 3%, 4%) was synthesized by a previously reported method.[20] A mixture comprising 1 mmol $LnCl_3 \cdot H_2O$ ($YbCl_3 \cdot H_2O$ and $TmCl_3 \cdot H_2O$), 6 mL oleic acid, and 15 mL 1-octadecene was loaded into a 50 mL round bottom flask. The mixture was stirred vigorously for 1 h at 160 °C to produce a clear solution with N_2 as the shielding gas. Then the solution was cooled down to 50 °C and a 10 mL methanol solution with NaOH (0.1 g) and NH_4F (0.148 g) was added, which was stirred for 30 min. The methanol and water in the mixture solution were evaporated at 100 °C with a strong stream of nitrogen to avoid oleic acid oxidized. The solution was heated to 300 °C and kept 60 min with constant stirring. Finally, the mixture was cooled down to room temperature and precipitated by ethanol. The synthesized $NaYb_{1-x}F_4:Tm_x^{3+}$ NPs were washed three times with a mixture of ethanol and cyclohexane to remove impurities. The NPs were then collected by centrifugation. After purification, the NPs were stored in cyclohexane.

The generation rate of ROS

The generation rate of reactive oxygen species can be evaluated by consumption rate of DPBF. The time-dependent concentration of DPBF during ROS generation can be described as follows:[21]

$$\frac{d[DPBF]}{dt} = -\sum_{i=1}^{n} k_i[ROS_i][DPBF] = -k[DPBF], \quad (2)$$

where [DPBF] and [ROS_i] are the concentrations of DPBF and ROS, respectively; k_i is the rate constant of chemical reaction between O_2 and DPBF; and k is the consumption rate of DPBF or the reciprocal of the time constant in the decrease of DPBF.

Eqn (2) can be rewritten as:

$$\ln\frac{[DPBF_0]}{[DPBF]} = kt. \quad (3)$$

Then, the consumption rate of DPBF (k) can be given by the slope of the eqn (3).

For the concentrations of DPBF, we employ the Beer–Lambert law to calculate. The transmission intensity can be described as:

$$I_t = I_0 \exp(\sigma[DPBF]L), \quad (4)$$

where I_t and I_0 are the transmission intensity with and without absorption by samples, σ is the absorption cross section of PS, and L is the optical path. Here, $A = \sigma[DPBF]L \propto [DPBF]$.

Therefore, A can be used to estimate the change of DPBF concentration, and is given by:

$$A = \ln(I_0/I_t) \quad (5)$$

Absorption spectra measurement

DPBF solution (0.02 μmol mL^{-1}) with $NaYb_{1-x}F_4:Tm_x^{3+}$ (12 μmol mL^{-1}) was exposed to a 980 nm laser with the power of 1.5 W. The transmission spectra of DPBF in the solutions were measured every 20 minutes. A deuterium lamp served as the light source of transmission spectra, and a miniature QE65000 fiber optic spectrometer (Ocean Optics, USA) was used to detect the transmission from UV to visible light. The absorption spectrum of DPBF can be obtained according to the Beer–Lambert law.

Characterization method

X-ray diffraction (XRD) was obtained using Rigaku D/MAX-2600/PC with the Cu Kα radiation ($\lambda = 1.5406$ Å) at the scanning step at 0.02°. Transmission electron microscope (TEM) image was obtained using FEI Tecnai TF20.

Fluorescence spectra measurement

The fluorescence spectra were measured at room temperature using 70 mW power-controlled 980 nm laser diode as an excitation source. A monochromator (Zolix Instrument SBP 300) coupled with photomultiplier (Zolix Instrument PMTH-S1-CR131) was used to collect the 800 nm upconversion fluorescence. The scanning step is 1 nm. All fluorescence spectra were measured using the same measuring system under the same conditions.

Conclusions

The ROS generation and 800 nm emission in $NaYb_{1-x}F_4:Tm_x^{3+}$ NPs were investigated for application in imaging-guided PDT. The Tm^{3+} doping concentration was found to have opposite effects on the ROS generation and 800 nm emission. At low Tm^{3+} concentrations, the increasing rate of ROS generation exceeded the decreasing rate of fluorescence intensity. Additionally, the former was slower than the latter. When the Tm^{3+} concentration reached 1%, the variation rate of ROS generation and fluorescence intensity was equal. At this concentration, the energy of Yb^{3+} in the excited state could be used efficiently and the combination effect of fluorescence imaging and PDT was optimum.

Conflicts of interest

There are no conflicts to declare.

Acknowledgements

This work was supported by the National Natural Science Foundation of China (no. 81571720 and 81530052), Natural Science Foundation of Heilongjiang Province (No. LH2019A028), the 13th Five-year Educational Science Planned Projects in Heilongjiang Province (No. GJB1319071).

References

1 A. V. Kachynski, A. Pliss, A. N. Kuzmin, T. Y. Ohulchanskyy, A. Baev, J. Qu and P. N. Prasad, *Nat. Photonics*, 2014, **8**, 455.
2 Fujin Ai, N. Wang, X. M. Zhang, T. Y. Sun, Q. Zhu, W. Kong, F. Wang and G. Y. Zhu, *Nanoscale*, 2018, **10**, 4432.
3 H. M. Chen, G. D. Wang, Y. J. Chuang, Z. P. Zhen, X. Y. Chen, P. Biddinger, Z. L. Hao, F. Liu, B. Z. Shen, Z. W. Pan and J. Xie, *Nano Lett.*, 2015, **15**, 2249.
4 Y. K. Wang, D. D. Cai, H. X. Wu, Y. Fu, Y. Cao, Y. J. Zhang, D. M. Wu, Q. W. Tian and S. P. Yang, *Nanoscale*, 2018, **10**, 4452.
5 M. Ochsner, *J. Photochem. Photobiol., B*, 1997, **39**, 1.
6 T. J. Dougherty, C. J. Gomer, B. W. Henderson, G. Jori, D. Kessel, M. Korbelik, J. Moan and Q. Peng, *J. Natl. Cancer Inst.*, 1998, **90**, 889.
7 M. Ethirajan, Y. H. Chen, P. Joshi and R. K. Pandey, *Chem. Soc. Rev.*, 2011, **40**, 340.
8 E. D. Sternberg, D. Dolphin and C. Bruckner, *Tetrahedron*, 1998, **54**, 4151.
9 M. Pawlicki, H. A. Collins, R. G. Denning and H. L. Anderson, *Angew. Chem., Int. Ed.*, 2009, **48**, 3244.
10 H. A. Collins, M. Khurana, E. H. Moriyama, A. Mariampillai, E. Dahlstedt, M. Balaz, M. K. Kuimova, M. Drobizhev, V. X. D. Yang, D. Phillips, A. Rebane, B. C. Wilson and H. L. Anderson, *Nat. Photonics*, 2008, **2**, 420.
11 B. M. Velusamy, J. Y. Shen, J. T. Lin, Y. C. Lin, C. C. Hsieh, C. H. Lai, C. W. Lai, M. L. Ho, Y. C. Chen, P. T. Chou and J. K. Hsiao, *Adv. Funct. Mater.*, 2009, **19**, 2388.
12 X. Liu, M. Zheng, X. Kong, Y. Zhang, Q. Zeng, Z. Sun, W. Buma and H. Zhang, *Chem. Commun.*, 2013, **49**, 3224.
13 S. Y. Liu, Y. Yuan, Y. K. Yang, Z. H. Liu, S. Y. Yin, W. P. Qin and C. F. Wu, *J. Mater. Chem. B*, 2017, **5**, 8169.
14 P. Zhang, W. Steelant, M. Kumar and M. Scholfield, *J. Am. Chem. Soc.*, 2007, **129**, 4526.
15 J. Y. Zhang, S. Chen, P. Wang, D. J. Jiang, D. X. Ban, N. Z. Zhong, G. C. Jiang, H. Li, Z. Hu, J. R. Xiao, Z. G. Zhang and W. W. Cao, *Nanoscale*, 2017, **9**, 2706.
16 J. Y. Zhang, H. Zhao, X. T. Zhang, X. Z. Wang, H. Gao, Z. G. Zhang and W. W. Cao, *J. Phys. Chem. C*, 2014, **118**, 2820.
17 H. J. Liang, Y. D. Zheng, L. Wu, L. X. Liu, Z. G. Zhang and W. W. Cao, *J. Lumin.*, 2011, **131**, 1802.
18 C. Z. Zhao, X. G. Kong, S. G. Song and X. K. Li, *Chin. J. Lumin.*, 2013, **34**, 959.
19 Y. Wang, K. Liu, X. M. Liu, K. Dohnalova, T. Gregorkiewicz, X. G. Kong, M. C. G. Aalders, W. J. Buma and H. Zhang, *J. Phys. Chem. Lett.*, 2011, **2**, 2083.
20 Z. Q. Li and Y. Zhang, *Nanotechnology*, 2008, **19**, 345606.
21 F. Wilkinson, W. P. Helman and A. B. Ross, *J. Phys. Chem. Ref. Data*, 1993, **22**, 113.